Chapter 17

Use of Thermal Infrared Imaging for Monitoring Renewed Dome Growth at Mount St. Helens, 2004

By David J. Schneider[1], James W. Vallance[2], Rick L. Wessels[1], Matthew Logan[2], and Michael S. Ramsey[3]

Abstract

A helicopter-mounted thermal imaging radiometer documented the explosive vent-clearing and effusive phases of the eruption of Mount St. Helens in 2004. A gyrostabilized gimbal controlled by a crew member housed the radiometer and an optical video camera attached to the nose of the helicopter. Since October 1, 2004, the system has provided thermal and video observations of dome growth. Flights conducted as frequently as twice daily during the initial month of the eruption monitored rapid changes in the crater and 1980–86 lava dome. Thermal monitoring decreased to several times per week once dome extrusion began. The thermal imaging system provided unique observations, including timely recognition that the early explosive phase was phreatic, location of structures controlling thermal emissions and active faults, detection of increased heat flow prior to the extrusion of lava, and recognition of new lava extrusion. The first spines, 1 and 2, were hotter when they emerged (maximum temperature 700°–730°C) than subsequent spines insulated by as much as several meters of fault gouge. Temperature of gouge-covered spines was about 200°C where they emerged from the vent, and it decreased rapidly with distance from the vent. The hottest parts of these spines were as high as 500°–730°C in fractured and broken-up regions. Such temperature variation needs to be accounted for in the retrieval of eruption parameters using satellite-based techniques, as such features are smaller than pixels in satellite images.

[1] U.S. Geological Survey, 4200 University Drive, Anchorage, AK 99508

[2] U.S. Geological Survey, 1300 SE Cardinal Court, Vancouver, WA 98683

[3] Department of Geology and Planetary Science, University of Pittsburgh, 200 SRCC Building, Pittsburgh, PA 15260

Introduction

Detection and measurement of elevated temperature can play an important role in understanding the processes involved with active volcanic processes. As magma moves into a volcano, an increase in surface heat flow may occur that is manifested by various phenomena, such as increases in fumarole temperatures, opening of new fumaroles, development of hot faults and fractures, increases in hot spring and crater lake temperatures, and melting of snow and ice. Once an eruption begins there are numerous potential heat sources such as eruption columns, lava lakes, lava domes, lava flows, and pyroclastic-flow deposits. Analysis of thermal data can provide a means to detect unrest, observe phenomena not discernible at visible wavelengths, see through thin cloud cover and steam, and track changes in eruption style and eruption volume.

Thermal data are acquired at a variety of spatial and temporal resolutions: (1) low spatial resolution (kilometer scale) from high temporal resolution (multiple images per day) satellite sensors such as GOES, AVHRR and MODIS (Dehn and others, 2002; Harris and others, 1997; Wright and others, 2002); (2) moderate spatial resolution (tens of meters) from low temporal resolution (weekly or greater) satellite sensors such as ASTER and Landsat TM/ETM+ (Flynn and others, 2001; Ramsey and Dehn, 2004; Vaughan and others, 2005); and (3) high spatial resolution (meter scale) from airborne or ground-based thermal imaging radiometers deployed on a tactical basis. This study focuses on an application of the latter—high-resolution thermal monitoring of eruptive activity at Mount St. Helens during October and November 2004.

The use of thermal imaging radiometers for monitoring volcanic activity has increased greatly over the past 5 years. A new generation of instruments that has entered the commercial marketplace utilizes detector arrays without external cooling (such as liquid nitrogen), thereby simplifying field logistics and increasing portability. These instruments provide calibrated temperature images and are useful in such applications

as detecting heated fractures prior to lava eruption (Andronico and others, 2005) or flank collapse (Calvari and others, 2005), estimation of lava effusion rate (Harris and others, 2005a), and study of eruption dynamics (Harris and others, 2005b; Patrick and others, in press).

The reawakening of Mount St. Helens in September 2004 began with a swarm of shallow earthquakes on September 23 (Moran and others, this volume, chap. 2) and progressed to deformation and cracking of glacier ice on the crater floor south of the 1980–86 dome to form the so-called welt, which was first observed on September 26 (Dzurisin and others, this volume, chap. 14). In response to this unrest, thermal-image monitoring began on October 1, 2004, to establish baseline thermal imagery and to examine the 1980–86 dome for signs of deformation. This paper reports results of the thermal surveys conducted during the first 2 months of activity during vent clearing and early stages of dome extrusion from October to December 2004. Thermal monitoring has continued throughout the eruption and has aided in the analysis of subsequent dome growth (Vallance and others, this volume, chap. 9).

Instrumentation and Methodology

The imaging system used in this study comprises a FLIR Systems ThermaCAM™ PM595 infrared camera and a Sony EVI-370 (visual-wavelength) video camera housed in a four-axis gyrostabilized gimbal that is mounted to the nose of a Bell-206 helicopter (fig. 1A). Although these types of thermal imaging cameras are generally referred to as FLIR, for Forward Looking Infrared, the gimbal can rotate in any direction. A crew member controls gimbal orientation and camera operation with a remote control (fig. 1B). The infrared camera utilizes a 320×240 microbolometer array that detects long-wave thermal radiation in the 7.5–13-μm atmospheric window and converts these values to brightness temperature. A 12°-wide telephoto lens provides a horizontal field of view of 210 m and a pixel resolution of 1.5 m at a distance of 1,000 m. Temperature is measured in three ranges,–40–200°C, 30°–800°C, and 350°–1,500°C. An internal flash memory card stores data from the infrared camera at 14-bit resolution and maximum frequency of 1 Hz. The visual video camera has a resolution of 720×480 pixels and a 12x auto-focus zoom lens. Analog video signals from the infrared and visual cameras are recorded simultaneously. These data are used to provide context and geographical reference for the individually calibrated thermal images.

The total radiant emittance measured by the infrared camera is

$$W_{tot} = \varepsilon\tau W_{obj} + (1 - \varepsilon)\, \tau W_{refl} + (1 - \tau)W_{atm}, \qquad (1)$$

where ε is the emissivity of the object (a measure of how much radiation is emitted from an object compared to a perfect blackbody emitter, see discussion), τ is the atmospheric transmission, W_{obj} is the emission from the object, W_{refl} is the reflected emission from ambient sources, and W_{atm} is the emission from the atmosphere. The camera system converts radiant emittance (as measured by camera detector voltage) to brightness temperature internally using factory-defined calibration coefficients. We use an average emissivity value of 0.96 based on laboratory measurements of a dacite reference (Vaughan and others, 2005). We use ThermaCAM™ Researcher software to calculate atmospheric transmissivity using measured values of the ambient air temperature, relative humidity, and atmospheric path length (from the object to the camera).

The telephoto capabilities of the infrared camera allowed for safe helicopter operations from outside the 1980 crater at a typical altitude of 3,000 m above sea level (600 m above the crater rim) and a horizontal distance of 1,000 m from the

Figure 1. Forward Looking Infrared (FLIR) thermal and visual video imaging system used during airborne observations of Mount St. Helens, 2004–2007. *A*, FLIR instrument mounted on nose of Bell 206-L helicopter. Inset shows infrared (top) and visual video (bottom) lenses. *B*, Remote control panel used to display infrared and visual video streams, to control orientation of sensors using a joystick, and to capture data.

welt on the south crater floor. This was especially important for flights conducted during the first week of October 2004 when there was a high level of uncertainty regarding eruption prognosis and associated hazard. Infrared images, digital still photographs, and infrared and visual video were collected primarily at an oblique perspective, in many cases allowing for observation under steam and gas plumes that would have been impossible from a vertical viewing perspective. The thermal infrared and visual video collected using this system also provided striking graphical images for distribution to the media (Driedger and others, this volume, chap. 24).

In this study, thermal images are displayed in pseudo-color. Minimum and maximum temperature values (shown by a scale bar) are selected to provide optimal image enhancement. In some cases, the maximum temperature value reported in the text is higher than the maximum value shown by the scale bar.

Observations

Vent Clearing

We began thermal infrared monitoring on October 1, 2004, to develop baseline thermal images of the 1980–86 dome, to investigate the uplifted welt on the south crater floor, and to determine whether there was any thermal evidence for fracturing or faulting in the 1980–86 dome in response to ongoing uplift. Imaging began at 1156 PDT and showed several warm fumarolic regions with temperatures of 40° to 65°C, primarily on the north flank of the dome, as well as the influence of solar heating on the south flank. The region of the dome and the south crater floor adjacent to the welt (an area of visible deformation and faulting) was near ambient temperature (0°–15°C) except for a t-shaped thermal lineament (figs. 2A, 2B) at the west end of the graben that formed during dome extrusion in 1985 near the area of the dome informally known as Opus. This lineament had temperatures of 30° to 38°C.

At approximately 1202 PDT an ash-rich explosion ruptured ice at the west end of the welt. This event began without recognizable precursory seismicity (Moran and others, this volume, chap. 6) and without any observable thermal change in images collected 15 seconds prior to onset. The eruption column comprised ballistic projectiles, jetting, ash-rich projections inclined northward, and a convecting steam-rich cloud (figs. 2C, 2D). The maximum temperature, 160°C, recorded from the base the column, indicated a phreatic rather than a magmatic mechanism. Infrared video shows that ballistic blocks were ejected primarily northward, where they destroyed seismic station SEP and GPS station DOM1 on the 1980–86 dome, located about 400 m north of the vent. Within 5 minutes of the eruption onset, a horizontally convecting ash-rich cloud developed and moved westward from the vent until it encountered the crater wall (figs. 2E, 2F). The steam-and-ash cloud ultimately reached an altitude of ~4,500 m above sea level. Ash emissions ended abruptly at 1220 PDT, and images collected several minutes later once the residual steam dispersed revealed a vent with a diameter of ~20 m in ice of the welt and a broad area of ash deposits on the west crater floor (fig. 2G). Vent temperatures were only slightly above freezing (2°–6°C). Deposits adjacent to the vent had temperatures that ranged from 45° to 50°C, and ballistic blocks with similar temperatures lay in small areas on the south and west flank of the 1980–86 dome (fig. 2H). The relatively low temperatures of the vent and deposits provide further evidence for a phreatic rather than magmatic eruption mechanism. A minor amount of snow and ice was melted, generating a small channelized flow that extended several hundred meters west from the vent.

Rapid deformation and uplift of the welt continued following the explosion, and thermal images tracked increasing temperatures of certain features (figs. 3, 4). Uplift of Opus (south of the 1985 graben) began to expose warmer interior rocks primarily on its eastern margin. Images of the Opus area collected on October 1, 2004 (figs. 3A, 3B), show several areas of elevated surface temperatures that ranged from 40° to 50°C. Thermal images taken the following day showed that this area had been uplifted further and was the source of nearly constant warm rockfalls. By October 3, a broad region of oxidized rock from the interior of the dome was exposed (fig. 3C), and warm rockfalls and streaks of elevated temperature were more pronounced (fig. 3D). An elongate region of elevated temperature, detected at the north margin of the welt, trended east to west along the axis of the 1985 graben and intersected the October 1 vent (figs. 4A, 4B). Areas of enhanced heat flow along normal faults appeared in images as shorter lineaments perpendicular to the 1985 graben (fig. 4B).

Three additional phreatic explosions on October 3, 4, and 5 (Moran and others this volume, chap. 6) indicated the presence of a shallow heat source. These events reamed out a small basin on the west end of the welt, wherein water and ice collected (fig. 5A). On October 4, small ash-rich geysers (less than 50 m high) erupted through the lake, after which hot upwelling gas bubbles with temperatures as high as 200°C appeared (fig. 5B). The last phreatic explosion on October 5 produced a new vent north of the earlier one. Over the next several days, new fumaroles developed near these vent regions, with temperatures as high as 55°C observed on October 7.

On October 10, after 2 days of poor weather, thermal imagery detected a broad steaming area of ice- and snow-free rock at the west end of the welt (fig. 6A). Elevated temperatures that ranged from 30° to 50°C characterized this broad area, and numerous hot point sources within it ranged from 100° to more than 270°C (fig. 6B). This marked increase in temperature was the greatest yet observed and presented strong evidence that magma was nearing the surface.

Lava Extrusion Begins

Lava, first observed on October 11, extruded from the northern part of the zone of elevated temperatures shown in
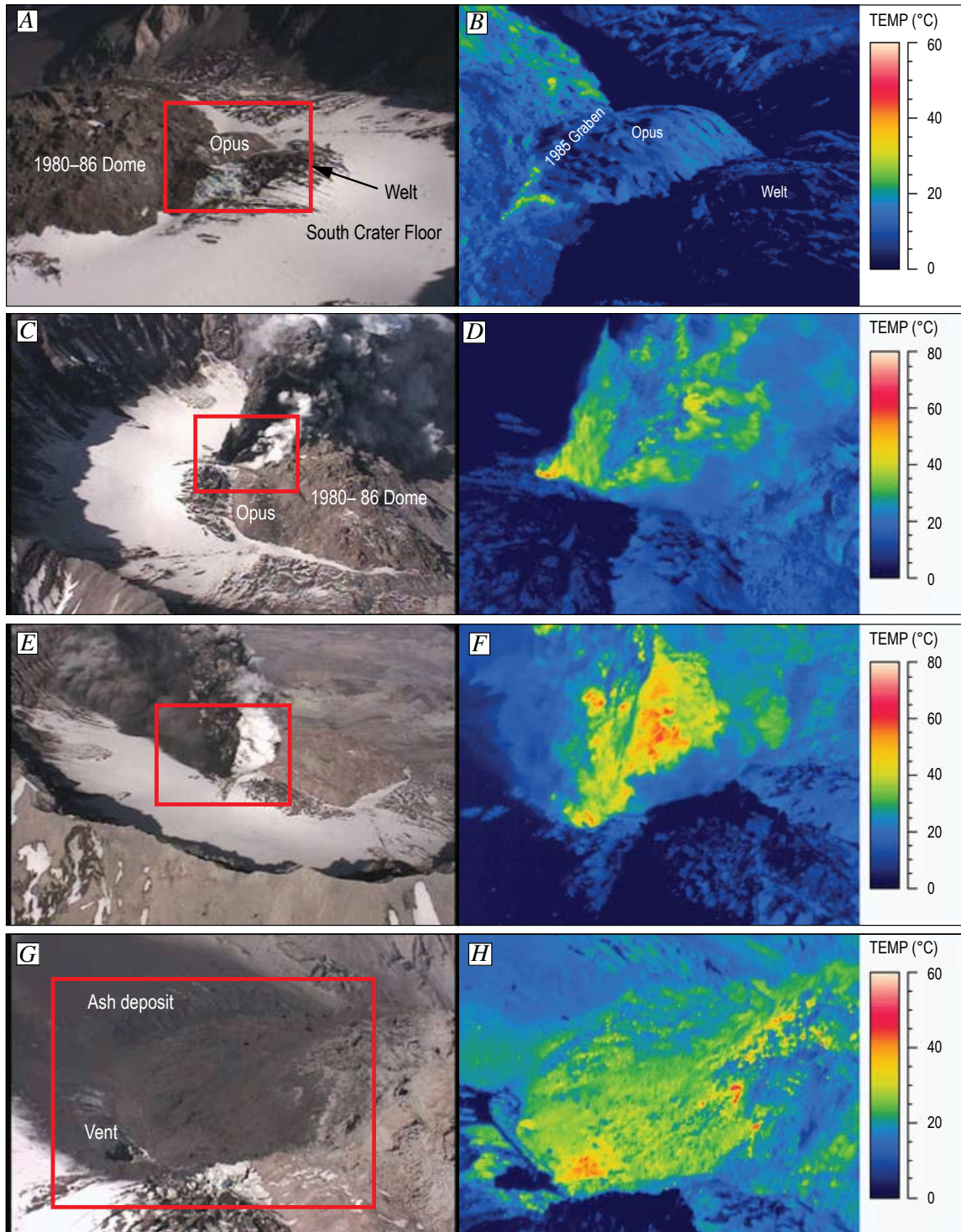
Figure 2. Comparisons between visual and infrared images of Mount St. Helens collected on October 1, 2004. Red rectangles in visual images show approximate boundaries of contemporaneous infrared images. *A*, Visual view from southwest of south crater floor and deforming welt collected at 11:56:30 PDT. *B*, Infrared image of area shown in *A*. *C*, Visual image from east showing phreatic eruption column collected at 12:05:50 PDT. *D*, Infrared image of area in *C*. *E*, Visual image from south showing phreatic eruption column collected at 12:07:07 PDT. *F*, Infrared image of area in *E*. *G*, Visual image from southeast showing vent region of phreatic explosion and associated ashfall deposits. *H*, Infrared image of area in *G*.
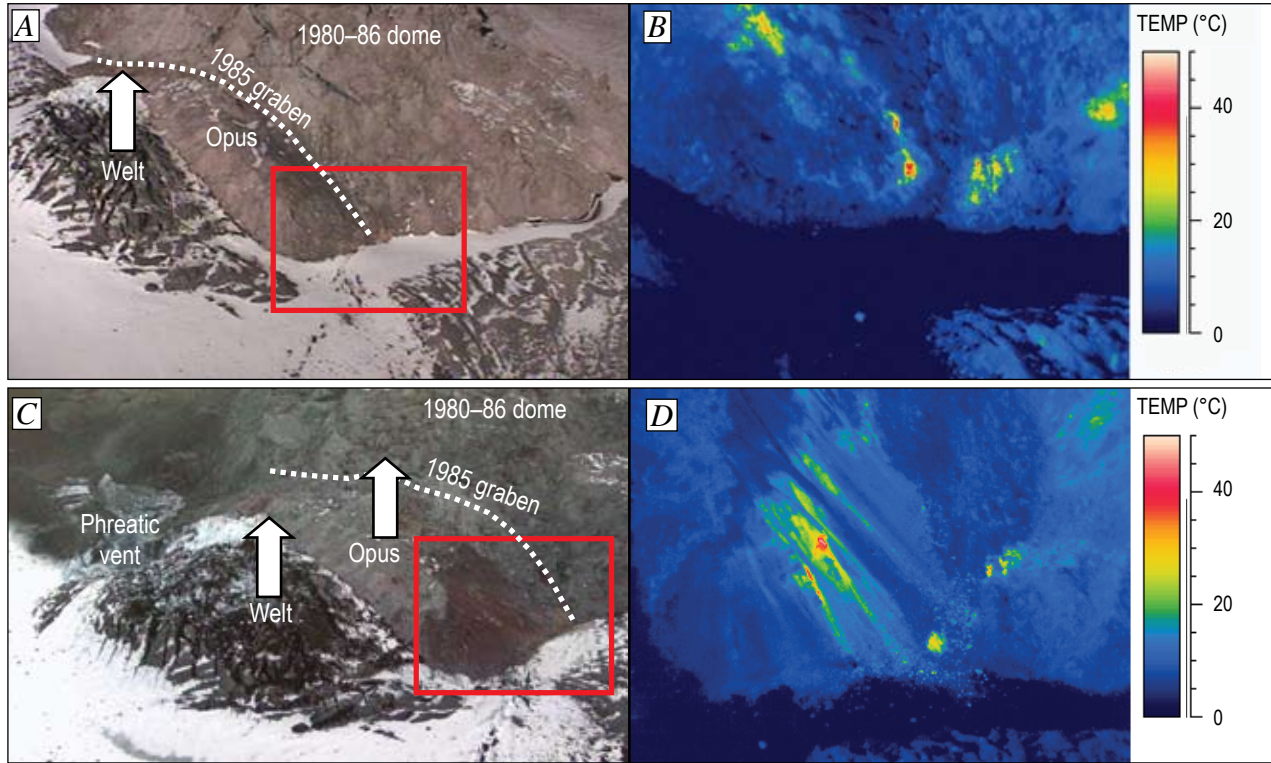
Figure 3. Comparisons between visual and infrared images of southeast part of 1980–86 dome and welt at Mount St. Helens. View from southeast. Red rectangles in visual images show approximate boundaries of contemporaneous infrared images. *A*, Visual image collected on October 1, 2004. *B*, Infrared image of area in *A*. *C*, Visual image collected on October 3, 2004. *D*, Infrared image of area in *C*.
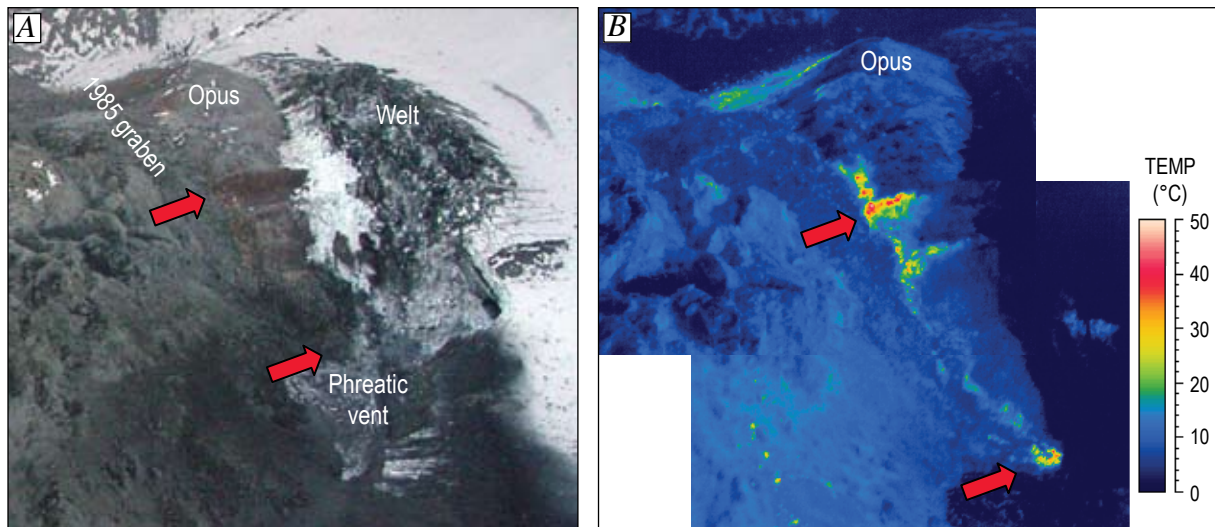

Figure 4. Comparison between visual and infrared images collected on October 3, 2004, of southern part of 1980–86 dome and welt at Mount St. Helens, showing thermal lineaments related to deformation. Red arrows indicate similar features between images. *A*, Visual image, view from the west. *B*, Contemporaneous infrared image.

figure 6. Following the usage of Cascades Volcano Observatory scientists, this and all subsequent lava extrusions are referred to as "spines" with a number assigned based on order of appearance. Spine 1 emerged as a fin-shaped slab approximately 80 m wide, 40 m high, and 10 m thick (fig. 7). Although the spine was partially obscured by steam during thermal observation (figs. 7A, 7C), temperatures as high as 580°C were measured at its base (figs. 7B, 7D). A small warm debris fan extended from spine 1, but there was little melting evident on adjacent snow and ice. Extrusion of spine 1 continued through at least October 14, with the hottest temperatures of the entire eruption sequence, 730°C, measured in cracks and fractures on that date.

Poor weather prevented thermal imaging flights from October 15 to 20, at which time extrusion of spine 2 had extended southward from spine 1 across the south crater floor. By October 24, spine 2 encountered the south crater wall (fig. 8). Spine 1 had cooled considerably since observation on October 14, with temperatures that ranged from 40° to 60°C where it emerged from the ground, whereas the temperature of spine 2 ranged as high as 430°C within fractured and fragmented rock near the likely zone of extrusion (fig. 8B). Intense steaming, caused by high relative humidity on this day (~80 percent), attenuated measured temperatures. The surfaces of spines 1 and 2 were rough, fractured, and blocky. Hot rockfalls on their west sides caused minor melting of snow and ice. An overflight on October 27 detected temperatures as hot as 700°C where spine 2 emerged, as well as a broad warm area in the debris cover southeast of spine 1. Observations were hampered by thick steam, but retrospective analysis suggests that extrusion of spine 3 had begun by this time.
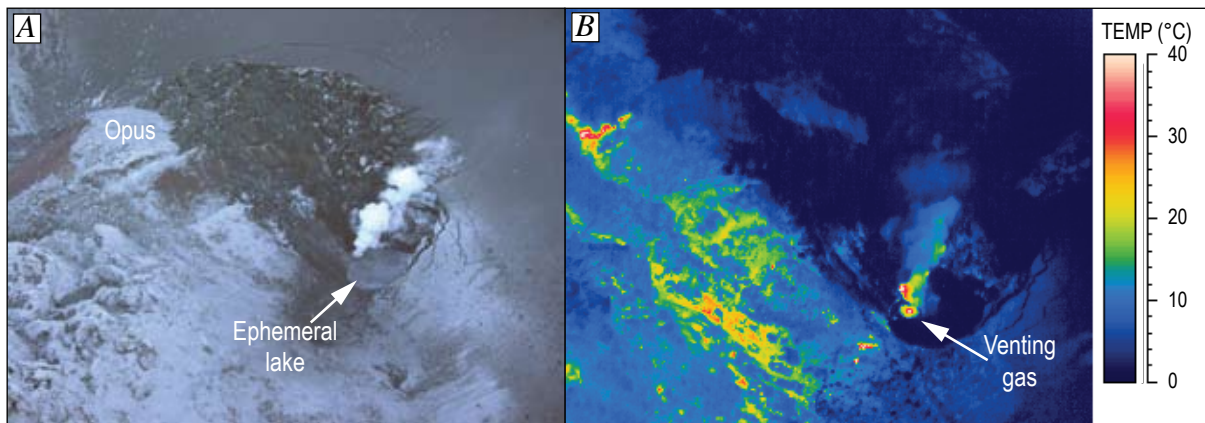

Figure 5.   Comparison between visual and infrared images collected on October 4, 2004, of southern part of 1980–86 dome and phreatic vent on welt at Mount St. Helens, showing hot gas venting through ephemeral lake. A, Visual image, view from west. B, Contemporaneous infrared image.
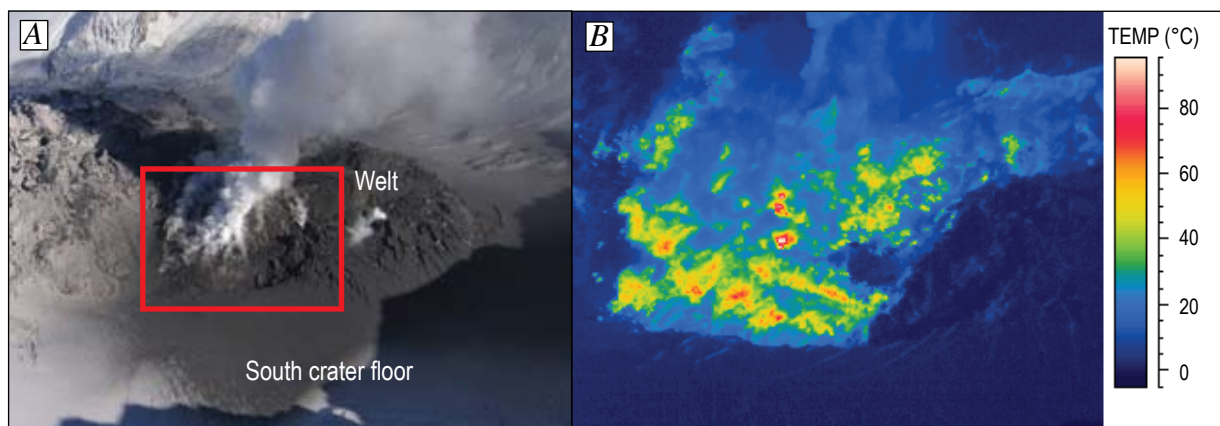

Figure 6.   Comparison between visual and infrared images collected on October 10, 2004, of welt at Mount St. Helens, showing increased heat flow due to magma nearing surface. View from west. Red rectangle in visual image shows approximate boundary of contemporaneous infrared image. A, Visual image. B, Infrared image.

By November 4, spine 3 had grown considerably. Its surface was smooth with a few large cracks (fig. 9A), but its west and south sides were blocky and fractured. As much as several meters of fault gouge covering spine 3 formed as largely crystallized magma ascended the upper part of the conduit (Cashman and others, this volume, chap. 19). Its smooth surface and recumbent attitude gave spine 3 a whaleback-like morphology. The fault gouge served as an effective insulator so that surface temperatures where it emerged from the vent on its north end ranged from 150° to 200°C and decreased exponentially to typical values of 25° to 50°C within 50 to 75 m (fig. 9B). The hottest temperature observed in small regions of collapse and fractures was 625°C.

Spine 3 moved toward the south as it was extruded and encountered the south crater wall by November 12 (Vallance and others, this volume, chap. 9). By late November, continued southward compression against the crater wall resulted in crumbling of spine 3 at its south end (fig 10A). Large open fractures in the fault-gouge carapace observed in thermal images (fig. 10B) suggested tensional cracking caused by bending of the solid spine as the extrusion continued southward. A typical temperature profile during this time period is shown in figure 11 along a line parallel to direction of extrusion. Temperature at the vent was typically 200°C and decreased abruptly southward, but was as high as 700°C in fractures.

Thermal infrared images continue to be used as a monitoring tool to observe dome growth and have documented the thermal characteristics of recumbent (whaleback) extrusion from November 2004 to April 2005, vertical spine extrusion from April to July 2005, and composite spine growth (composed of massive rock and disintegrating rock debris) from July 2005 to present (April 2007) (Vallance and others, this volume, chap. 9).

Discussion

Sources of Temperature Measurement Error

Accurate measurement of temperature using a thermal radiometer depends on several factors including viewing angle, characteristics of the atmospheric path, absorption by volcanic gases (water and SO_2), and the emissivity of the
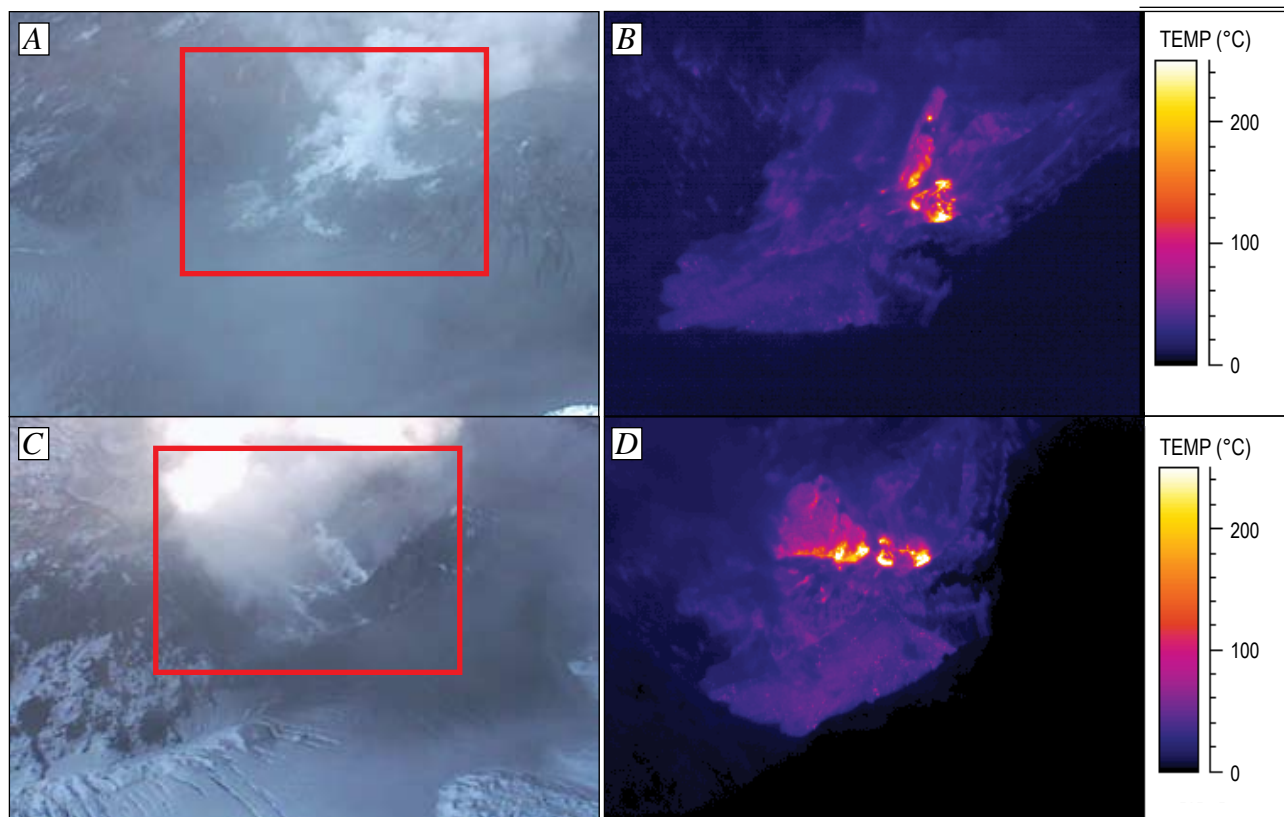

Figure 7.   Comparison between visual and infrared images of Mount St. Helens collected on October 11, 2004, showing the first views of lava at the surface. Red rectangle in visual image shows approximate boundary of contemporaneous infrared image. A, Visual image, view from southwest. B, Infrared image, view from southwest. C, Visual image, view from northwest. D, Infrared image, view from northwest.

target (Ball and Pinkerton, 2006). The maximum temperature values reported herein are most strongly affected by viewing angle, because the source of heat typically was a fracture or fissure. In these cases, physical blockage of the source(s) of thermal emission occurred, and imaging of the target from
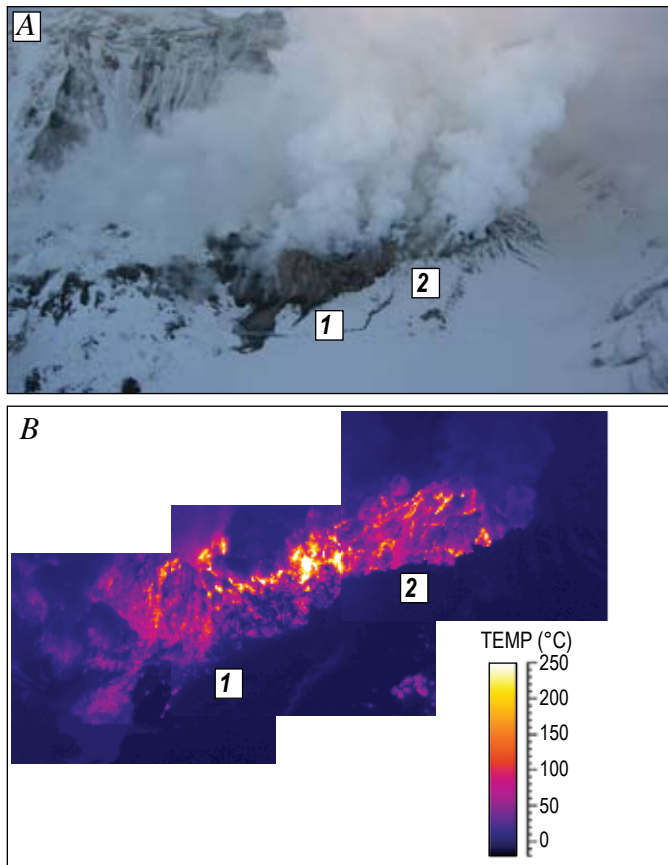
multiple viewing angles was required to detect the maximum values. In other cases, opaque steam clouds completely obscured the source, making it impossible to measure the temperature accurately.

Corrections for atmospheric-path absorption were made using ThermaCAM™ Researcher software and estimates of atmospheric temperature, relative humidity, and path length. For each mission, temperature and humidity values for Mount St. Helens were estimated using archived EDAS40 model sounding data provided by the NOAA Air Resources Laboratory (http//www.arl.noaa.gov/ready/amet.html). These values were used to compute the atmospheric transmission; the relation between these parameters is shown in figure 12 for a typical range of values. Uncertainty in estimating a representative relative humidity will contribute to a larger error in calculating transmission as the temperature of the atmosphere increases; the error will be compounded as the path length increases. Many of the thermal imaging missions were conducted at atmospheric temperatures near 0°C, the relative humidity values varied by a maximum of ±15 percent, and variation in path length was ±250 m. This results in a variation in atmospheric transmission of about ±2 percent. For an object with a temperature of 500°C, this results in a variation of ±10°C.

Although water is the dominant volcanic gas that absorbs infrared radiation, SO_2 has two strong absorption features (centered at wavelengths of 7.3 and 8.5 μm) within the spectral range of the thermal radiometer. Although techniques to quantify the systematic error in ground-based thermal infrared measurements caused by gas absorption are still being developed, it may be a significant issue in situations where gas concentrations are high (Sawyer and others, 2005). The SO_2 emission rates during the time period of this study were low, ranging from values at the lower detection limit of 1 metric ton per day (t/d) through October 4 and increasing to an average value of approximately 100 t/d thereafter (Gerlach and others, this volume, chap. 26). Thus, absorption of infrared emissions by SO_2 is likely to be a relatively small source of error.

Figure 8.   Comparison between visual and infrared images of Mount St. Helens collected on October 24, 2004, showing the development of spines 1 and 2 (as labeled). *A*, Visual image, view from the west. *B*, Composite infrared image.
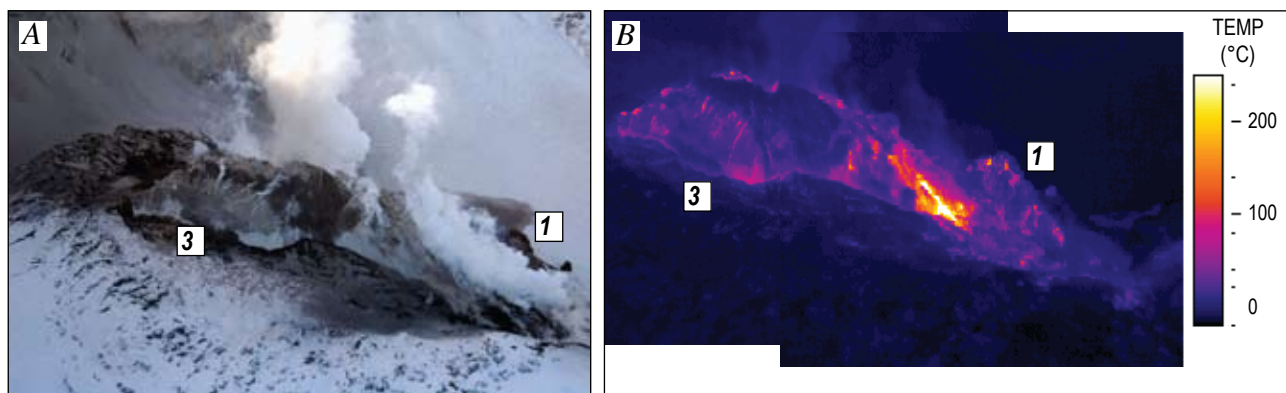

Figure 9.   Comparison between visual and infrared images of Mount St. Helens collected on November 4, 2004, showing the development of spines 1 and 3 (as labeled). *A*, Visual image, view from the northeast. *B*, Composite infrared image.

Emissivity is a measure of how much energy is emitted from an object compared to a theoretical perfect emitter known as a blackbody. In nature, all materials emit less energy than a blackbody, because energy is absorbed by the vibration of molecular bonds. They are referred to as selective radiators wherein emissivity varies as a function of wavelength. Although the emissivity of silicate rocks has a characteristic decrease in emissivity at a wavelength range of 8 to 10 μm, an average value over the broader range of 7.5 to 13 μm is used where measuring temperatures with a broadband radiometer. Variations in emissivity can also occur for a given rock type as a result of vesicularity and particle size. In general, emissivity decreases as vesicularity decreases (Ramsey and Fink, 1999). The 2004 lava was largely degassed and dense (Pallister and others, this volume, chap. 30), suggesting that the actual emissivity may be lower than a laboratory reference. Furthermore, very fine grained silicates (<60 μm) exhibit a decrease in emissivity at wavelengths above 11 μm, owing to scattering of radiant energy (Ramsey and Christensen, 1998). It is possible that ash fallout and (or) the cover of the chalky fault-gouge carapace served to reduce the effective emissivity of the extruded lava (compared to the dacite reference value). The effect of an overestimated emissivity would be an increase in the temperatures above those reported herein. The result of a variation in emissivity was tested by changing the value by a factor of 0.1 within the ThermaCAM™ Researcher software, which resulted in a change in temperature on the order of 20°C for an area with a temperature of 450°C. Thus, variations in emissivity may account for changes on the order of 5 percent in the absolute temperature recorded.
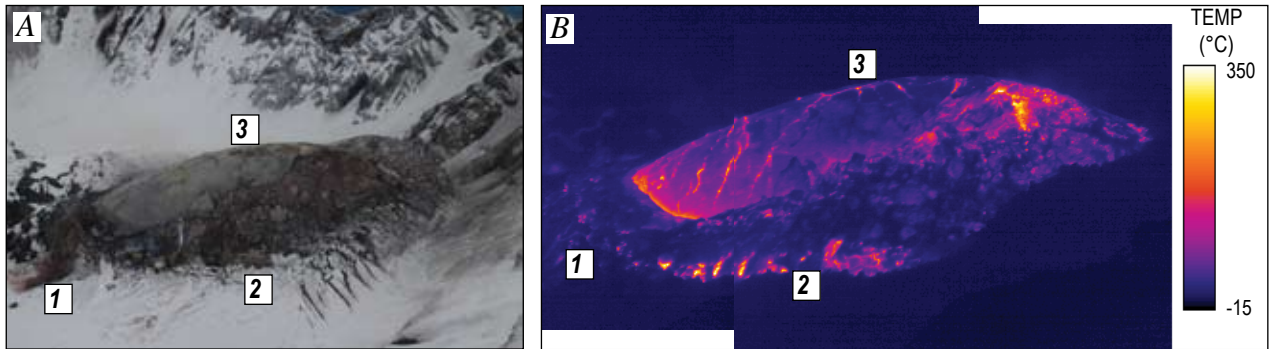

Figure 10. Comparison between visual and infrared images of Mount St. Helens collected on November 29, 2004, showing the development of spines 1 to 3. Spine 3 (as labeled) is actively being extruded and is crumbling as it encounters the south crater wall. A, Visual image, view from the west. B, Composite infrared image.
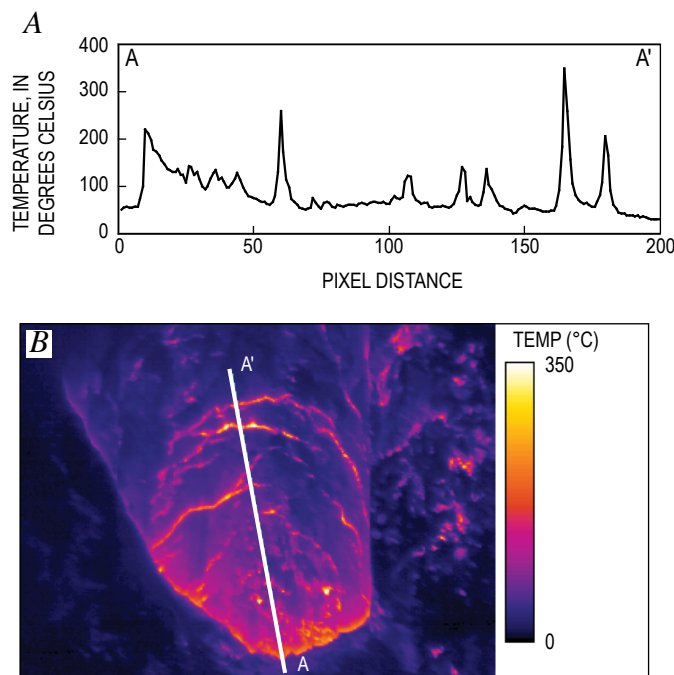

Figure 11. Temperature profile along north end of spine 3 at Mount St. Helens on November 29, 2004, showing typical temperatures observed during extrusion of whaleback spines. A, Temperature profile A–A'; profile length approximately 125 m, north toward left. B, Infrared image of spine 3 viewed from the north showing the location of the north-south profile, A–A'.

Thermal Imaging as a Response Tool

The rapid pace of unrest associated with the reawakening of Mount St. Helens in September 2004 resulted in an intense monitoring response by the Cascades Volcano Observatory (CVO) and the broader U.S. Geological Survey Volcano Hazards Program (VHP). Although handheld thermal imaging cameras have been used successfully in eruption response by other volcano observatories worldwide (Kauahikaua and others, 2003; Andronico and others, 2005; Calvari and others, 2005; Harris and others, 2005a), the gimbal-mounted system used during this response was a relatively new tool for VHP scientists. It had been flown on several missions at the Alaska Volcano Observatory (AVO) to collect baseline thermal data and on one flight in response to unrest at Mount Spurr (Power, 2004). Thus, the gimbal-mounted instrument was largely untested for eruption response by the USGS when first flown at Mount St. Helens on October 1, 2004; arriving only 6 minutes prior to the initial phreatic explosion. The utility of the instrument was quickly recognized as it was determined rapidly that the initial explosion was of phreatic origin. This information was quickly radioed to the operations center at CVO and used to apprise land management and emergency response personnel. In addition, the thermal and visual video imagery was made available to the media and was broadcast widely. The ability to control the gimbal and shoot video in a wide range of orientations was extremely useful as the helicopter maneuvered in response to the eruption cloud, topographic barriers, and wind. The telephoto capabilities were also vital, allowing for observation at a safe distance beyond the crater rim.

In addition to documenting thermal features on the crater floor and dome, use of the instrument during the first 2 weeks of October provided opportunities to test thermal-observation strategies and to determine what kinds of useful information could be obtained. The stability of the 1980–86 dome in response to the deformation on the south crater floor was initially of great concern, as potential eruption scenarios were evaluated involving (1) large-scale collapse of the 1980s dome toward the northern open end of the 1980 crater and (2) potential hazards to the public who had come to view the volcano. Thus, an important early use of the system was to look for the thermal expression of faults or fractures on the northern flank of the dome. Observations made throughout the current eruption have shown no significant change in thermal response of the 1980–86 dome and thus have eased concerns about its stability.

Structural Control of Heat Emissions

The south flank of the 1980–86 dome, which formed the northern part of the welt, showed several examples of structural control of heat emissions during a time of rapid uplift, faulting, and deformation (figs. 3, 4) along a graben formed during an episode of dome growth in 1985. Between flights on October 1 and 2, rapid uplift of tens of meters on the east end of the graben caused warm rockfalls from the newly exposed interior of the dome. Over the next several days, the thermal imaging system was able to record continued uplift in this region as expressed by displacement of thermal features and nearly continuous warm rockfalls. On the west end of the graben (fig. 4), the thermal expression of normal faulting was observed, suggesting that this area was not moving upward as rapidly as the east end. Although these features can be seen in visible images, the advantage of the thermal system was to highlight areas of interest during a time period of very rapid changes in surface topography. Similar phenomena (on a larger scale) were observed at Mount St. Helens in April and May 1980 during development of the bulge. For example, Kieffer and others (1981) documented increased heat flow from several faults, fractures, and brecciated zones using a variety of thermal imaging devices, and reported temperature values
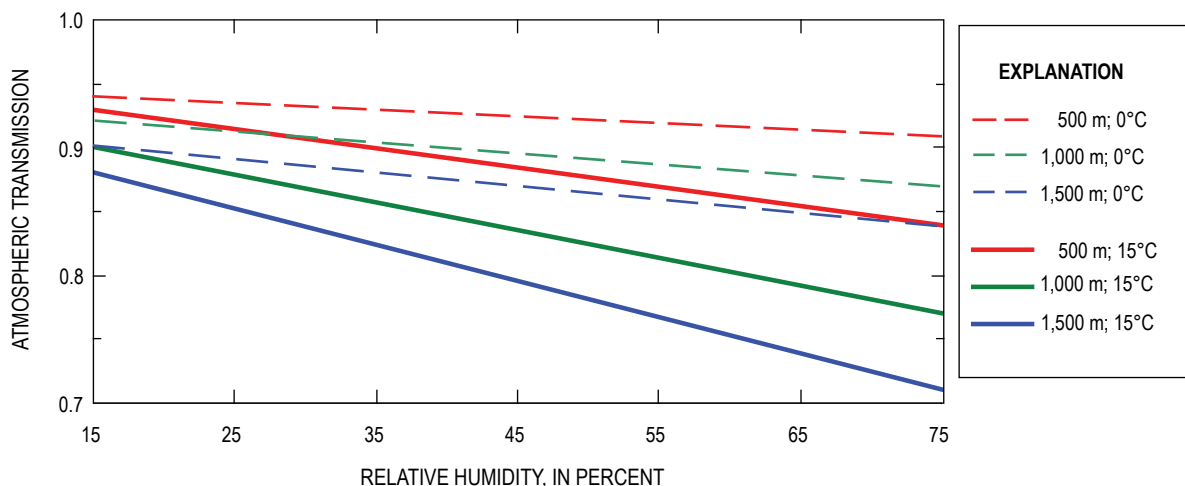

Figure 12.   Atmospheric transmission as a function of relative humidity, atmospheric temperature, and path length.

in these regions of 15° to >25°C above background, similar to those observed in October 2004. Structural control of heat emissions have also been noted at Mt. Etna in 2002 where hot fractures were observed several weeks prior to the eruption of a lava flow (Andronico and others, 2005), at Stromboli in 2002 where fractures were observed several hours prior to a major slope failure (Calvari and others, 2005), and at Augustine Volcano in 2006 where hot fractures and fissures were observed in the weeks preceding vulcanian explosions (D. Schneider, unpub. data). These studies suggest the broad utility of thermal imaging systems for detecting and monitoring deformation in the weeks and months prior to eruption.

The thermal measurements at Mount St. Helens documented an increase in heat flow on October 10 as magma neared the surface. On October 11, they provided unambiguous confirmation that lava (rather than uplifted crater floor) was being extruded. The imaging capabilities provided better viewing conditions at times when steam otherwise obscured observation (fig. 7) and allowed for an estimate of the volume of spine 1. The maximum temperature observed in fractures and regions of collapse during the eruption sequence was 730°C, well below the solidus temperature of dacite. Although the thermal measurements may underestimate the maximum temperature as a result of thermal stratification due to radiative cooling, the observations are consistent with the petrologic (Pallister and others, this volume, chap. 30; Cashman and others, this volume, chap. 19) and seismic observations (Moran and others, this volume, chap. 2) that suggest a viscous to solid transition at a depth of approximately 1 km.

Comparisons to Satellite Methods

The detection limit of satellite-based measurements of thermal emissions is largely a matter of spatial resolution. With the exception of large thermal features (such as lava lakes, crater lakes, and pyroclastic-flow deposits), most sources of volcanogenic heat are subpixel in size when viewed with moderate-resolution sensors such as ASTER (90-m pixels) or coarse-resolution sensors such as AVHRR or MODIS (1-km pixels). Thus, the signal detected by the satellite is a pixel-integrated value of (at least) a hot and a cold (background) component. In order for a thermal anomaly to be detected, the proportion of hot material within a pixel, or the temperature of the hot component, needs to increase to the point where the integrated temperature exceeds a threshold (compared to neighboring pixels). So it follows that the smaller the spatial resolution of a sensor, the more sensitive it will be to detecting anomalous pixels.

Vaughan and Hook (2006) examined nighttime (to eliminate the solar reflected radiance) ASTER thermal infrared data for Mount St. Helens and reported that a single-pixel, weak (10°C) thermal feature was observed on the evening of October 1 approximately 11 hours after the first phreatic explosion. They noted that this value was within the range of typical ASTER-derived temperatures observed over the

previous 5 years and would likely have not been viewed as significant without knowledge of the explosion. The next clear nighttime ASTER image was collected in February 2005 and showed an unambiguous maximum temperature of about 50°C. Although this instrument has been used successfully to monitor eruptive activity at many other volcanoes, the long period of time between successful, cloud-free nighttime images illustrates that significant eruptive activity can occur without being observed.

Manual analyses conducted by AVO of mid-infrared data from the AVHRR and MODIS sensors (1-km spatial resolution with multiple image collections per day) were not able to detect any unusual thermal (or volcanic ash) emissions during the precursory and vent-clearing phases of the eruption. The first weak thermal anomaly of 10°C (above background) was observed in data collected on the evening of October 11, shortly after the first observations of lava extrusion using the thermal imaging system (Alaska Volcano Observatory, unpub. data). It is unclear whether this level of activity would have been observed or reported without the knowledge of lava being extruded, as thermal anomalies of this magnitude can be masked by noise or other environmental factors. Thermal anomalies of 10° to 20°C above background were reported by AVO throughout most of October during times of clear weather and increased to a one-pixel anomaly of 32°C above background in nighttime data on November 8 (Alaska Volcano Observatory, unpub. data). This observation corresponds most closely with the thermal image shown in figure 9 and occurred about 2 weeks after the start of the extrusion of spine 3. By comparison, MODVOLC, an automated global system designed to detect volcanic activity (with a rather high threshold to reduce false alarms) (Wright and others, 2004), did not trigger until December 18. By this time, spine 3 had encountered the south crater wall and started to disintegrate. Undoubtedly the detection of thermal activity by satellite techniques was greatly reduced by the insulating properties of the relatively cool fault-gouge carapace. Once the spines grew large and began to break apart, detection was more apparent. Still, lava extrusion was ongoing for a least a month before satellite methods utilizing 1-km-resolution data were able to unambiguously detect it.

Conclusions

The use of airborne thermal imaging to document eruptive activity at Mount St. Helens began in October 2004 to develop baseline thermal images of the 1980–86 dome and to investigate the rising welt on the south crater floor. Since that time, it has become a routine monitoring tool for tracking evolution of the lava dome (Vallance and others, this volume, chap. 9). Some of the unique information that has been derived from these data to date include (1) rapid identification of the phreatic nature of the early vent-clearing explosive phase; (2) observation of the structural control of heat flow during times

of large-scale deformation of the south flank of the 1980–86 dome, which was part of the welt; (3) observations of the venting of hot gas through an ephemeral crater lake and increased heat flow through the welt, indicative of a shallow magma source; (4) confirmation of new lava reaching the surface; (5) characterization of the change in surface temperature of the lava spines, from the initial, hotter spines 1 and 2 that were free of fault gouge, to the cooler gouge-covered whaleback spines (beginning with spine 3); (6) documentation that the relatively low maximum temperature of 730°C agreed with petrologic and seismic data suggesting a viscous-to-solid transition at shallow depth; and (7) identification of the source of active lava extrusion, dome collapse, and large variation in surface temperatures. Such temperature variation needs to be accounted for in the retrieval of eruption parameters using satellite-based techniques, because the thermal features are of subpixel size in satellite images.

Acknowledgments

References Cited

Andronico, D., Branca, S., Calvari, S., Burton, M., Caltabiano, T., Corsaro, R.A., Del Carlo, P., Garfì, G., Lodato, L., Miraglia, L., Murè, F., Neri, M., Pecora, E., Pompilio, M., Salerno, G., and Spampinato, L., 2005, A multi-disciplinary study of the 2002–03 Etna eruption; insights into a complex plumbing system: Bulletin of Volcanology, v. 67, no. 4, p. 314–330, doi:10.1007/s00445-004-0372-8.

Ball, M., and Pinkerton, H., 2006, Factors affecting the accuracy of thermal imaging cameras in volcanology: Journal of Geophysical Research, v. 111, no. B11, B11203, 14 p., doi:10.1029/2005JB003829.

Calvari, S., Spampinato, L., Lodato, L., Harris, A.J.L., Patrick, M.R., Dehn, J., Burton, M.R., and Andronico, D., 2005, Chronology and complex volcanic processes during the 2002–2003 flank eruption at Stromboli volcano (Italy) reconstructed from direct observations and surveys with a handheld thermal camera: Journal of Geophysical Research, v. 110, no. B2, p. 1–23, doi:10.1029/2004JB003129.

Cashman, K.V., Thornber, C.R., and Pallister, J.S., 2008, From dome to dust; shallow crystallization and fragmentation of conduit magma during the 2004–2006 dome extrusion of Mount St. Helens, Washington, chap. 19 of Sherrod, D.R., Scott, W.E., and Stauffer, P.H., eds., A volcano rekindled; the renewed eruption of Mount St. Helens, 2004–2006: U.S. Geological Survey Professional Paper 1750 (this volume).

Dehn, J., Dean, K.G., Engle, K., and Izbekov, P., 2002, Thermal precursors in satellite images of the 1999 eruption of Shishaldin Volcano: Bulletin of Volcanology, v. 64, no. 8, p. 525–534, doi:10.1007/s00445-002-0227-0.

Driedger, C.L., Neal, C.A., Knappenberger, T.H., Needham, D.H., Harper, R.B., and Steele, W.P., 2008, Hazard information management during the autumn 2004 reawakening of Mount St. Helens volcano, Washington, chap. 24 of Sherrod, D.R., Scott, W.E., and Stauffer, P.H., eds., A volcano rekindled; the renewed eruption of Mount St. Helens, 2004–2006: U.S. Geological Survey Professional Paper 1750 (this volume).

Dzurisin, D., Lisowski, M., Poland, M.P., Sherrod, D.R., and LaHusen, R.G., 2008, Constraints and conundrums resulting from ground-deformation measurements made during the 2004–2005 dome-building eruption of Mount St. Helens, Washington, chap. 14 of Sherrod, D.R., Scott, W.E., and Stauffer, P.H., eds., A volcano rekindled; the renewed eruption of Mount St. Helens, 2004–2006: U.S. Geological Survey Professional Paper 1750 (this volume).

Flynn, L.P., Harris, A.J.L., and Wright, R., 2001, Improved identification of volcanic features using Landsat 7 ETM+: Remote Sensing of Environment, v. 78, nos. 1–2, p. 180–193.

Gerlach, T.M., McGee, K.A., and Doukas, M.P., 2008, Emission rates of CO_2, SO_2, and H_2S, scrubbing, and preeruption excess volatiles at Mount St. Helens, 2004–2005, chap. 26 of Sherrod, D.R., Scott, W.E., and Stauffer, P.H., eds., A volcano rekindled; the renewed eruption of Mount St. Helens, 2004–2006: U.S. Geological Survey Professional Paper 1750 (this volume).

Harris, A.J.L., Keszthelyi, L., Flynn, L.P., Mouginis-Mark, P.J., Thornber, C., Kauahikaua, J., Sherrod, D., Trusdell, F., Sawyer, M.W., and Flament, P., 1997, Chronology of the episode 54 eruption at Kilauea Volcano, Hawaii, from GOES-9 satellite data: Geophysical Research Letters, v. 24, no. 24, p. 3281–3284.

Harris, A., Dehn, J., Patrick, M., Calvari, S., Ripepe, M., and Lodato, L., 2005a, Lava effusion rates from hand-held thermal infrared imagery: an example from the June 2003 effusive activity at Stromboli: Bulletin of Volcanology, v. 68, no. 2, p. 107–117, doi:10.1007/s00445-005-0425-7.

Harris, A., Ripepe, M., Sahetapy-Engel, S., Marchetti, E., and Patrick, M., 2005b, Plume ascent velocities measured during explosive eruptions using thermal infrared thermometers [abs.]: Eos (American Geophysical Union Transactions), v. 86 no. 52, Fall Meeting Supplement, Abstract V24A-06.

Kauahikaua, J., Sherrod, D.R., Cashman, K.V., Heliker, C.,

Hon, K., Mattox, T.N., and Johnson, J.A., 2003, Hawaiian lava-flow dynamics during the Puʻu ʻŌʻō-Kūpaianaha eruption; a tale of two decades, *in* Heliker, C., Swanson, D.A., and Takahashi, T.J., eds., The Puʻu ʻŌ ʻō -Kūpaianaha eruption of Kīlauea Volcano, Hawaiʻi; the first 20 years: U.S. Geological Survey Professional Paper 1676, p. 63–87.

Kiefer, H.H., Frank, D., and Friedman, J.D., 1981, Thermal infrared surveys at Mount St. Helens—observations prior to the eruption of May 18, *in* Lipman, P.W., and Mullineaux, D.R., eds., The 1980 eruptions of Mount St. Helens, Washington: U.S. Geological Survey Professional Paper 1250, p. 257–277.

Moran, S.C., Malone, S.D., Qamar, A.I., Thelen, W.A., Wright, A.K., and Caplan-Auerbach, J., 2008a, Seismicity associated with renewed dome building at Mount St. Helens, 2004–2005, chap. 2 *of* Sherrod, D.R., Scott, W.E., and Stauffer, P.H., eds., A volcano rekindled; the renewed eruption of Mount St. Helens, 2004–2006: U.S. Geological Survey Professional Paper 1750 (this volume).

Moran, S.C., McChesney, P.J., and Lockhart, A.B., 2008b, Seismicity and infrasound associated with explosions at Mount St. Helens, 2004–2005, chap. 6 *of* Sherrod, D.R., Scott, W.E., and Stauffer, P.H., eds., A volcano rekindled; the renewed eruption of Mount St. Helens, 2004–2006: U.S. Geological Survey Professional Paper 1750 (this volume).

Pallister, J.S., Thornber, C.R., Cashman, K.V., Clynne, M.A., Lowers, H.A., Mandeville, C.W., Brownfield, I.K., and Meeker, G.P., 2008, Petrology of the 2004–2006 Mount St. Helens lava dome—implications for magmatic plumbing and eruption triggering, chap. 30 *of* Sherrod, D.R., Scott, W.E., and Stauffer, P.H., eds., A volcano rekindled; the renewed eruption of Mount St. Helens, 2004–2006: U.S. Geological Survey Professional Paper 1750 (this volume).

Patrick M.R., Harris, A.J.L., Ripepe, M., Dehn, J., Rothery, D.A., and Calvari, S., 2007, Strombolian explosive styles and source conditions; insights from thermal (FLIR) video: Bulletin of Volcanology, v. 69, no. 7, p. 769-784, doi:10.1007/s00445-006-0107-0.

Power, J., 2004, Renewed unrest at Mount Spurr volcano, Alaska [abs.]: Eos (American Geophysical Union Transactions), v. 85, no. 43, p. 434.

Ramsey, M.S., and Christensen, P.R., 1998, Mineral abundance determination; Quantitative deconvolution of thermal emission spectra: Journal of Geophysical Research, v. 103, no. B1, p. 577–596.

Ramsey, M., and Dehn, J., 2004, Spaceborne observations of the 2000 Bezymianny, Kamchatka, eruption; the integration of high-resolution ASTER data into near real-time monitoring using AVHRR: Journal of Volcanology and Geothermal Research, v. 135, nos. 1–2, p. 127–146, doi:10.1016/j.jvolgeores.2003.12.014.

Ramsey, M.S., and Fink, J.H., 1999, Estimating silicic lava vesicularity with thermal remote sensing; a new technique for volcanic mapping and monitoring: Bulletin of Volcanology, v. 61, no. 1, p. 32–39.

Sawyer, G., Burton, M., and Oppenheimer, C., 2005, The effect of volcanic gases on quantitative temperature measurements using the FLIR thermal camera [abs.]: Eos (American Geophysical Union Transactions), v. 86, no. 52, Fall Meeting Supplement, Abstract V24A-08.

Vallance, J.W., Schneider, D.J., and Schilling, S.P., 2008, Growth of the 2004–2006 lava-dome complex at Mount St. Helens, Washington, chap. 9 *of* Sherrod, D.R., Scott, W.E., and Stauffer, P.H., eds., A volcano rekindled; the renewed eruption of Mount St. Helens, 2004–2006: U.S. Geological Survey Professional Paper 1750 (this volume).

Vaughan, R.G., and Hook, S.J., 2006, Using satellite data to characterize the temporal thermal behavior of an active volcano; Mount St. Helens, WA: Geophysical Research Letters, v. 33, L20303, doi:10.1029/2006GL027957.

Vaughan, R.G., Hook, S.J., Ramsey, M.S., Realmuto, V.J., and Schneider, D.J., 2005, Monitoring eruptive activity at Mount St. Helens with TIR image data: Geophysical Research Letters, v. 32, L19305, doi:10.1029/2005GL024112.

Wright, R., Flynn, L., Garbeil, H., Harris, A., and Pilger, E., 2002, Automated volcanic eruption detection using MODIS: Remote Sensing of Environment, v. 82, no. 1, p. 135–155.

Wright, R., Flynn, L.P., Garbeil, H., Harris, A.J.L., and Pilger, E., 2004, MODVOLC: Near-real-time thermal monitoring of global volcanism: Journal of Volcanology and Geothermal Research, v. 135, nos. 1–2, p. 29–49.